Mon. Not. R. Astron. Soc. **000**, 000–000 (0000) Printed 5 February 2008 (MN LATEX style file v2.2)

Extended inverse-Compton emission from distant, powerful radio galaxies

M. C. Erlund,[1⋆] A. C. Fabian,[1] Katherine M. Blundell,[2] A. Celotti[3] and C. S. Crawford[1]

[1]*Institute of Astronomy, Madingley Road, Cambridge CB3 0HA*
[2]*University of Oxford, Astrophysics, Denys Wilkinson Building, Keble Road, Oxford OX1 3RH*
[3]*SISSA/ISAS, via Beirut 4, 34014 Trieste, Italy*

5 February 2008

ABSTRACT

We present *Chandra* observations of two relatively high redshift FR II radio galaxies, 3C 432 and 3C 191 ($z = 1.785$ and $z = 1.956$ respectively), both of which show extended X-ray emission along the axis of the radio jet or lobe. This X-ray emission is most likely to be due to inverse-Compton scattering of Cosmic Microwave Background (CMB) photons. Under this assumption we estimate the minimum energy contained in the particles responsible. This can be extrapolated to determine a rough estimate of the total energy. We also present new, deep radio observations of 3C 294, which confirm some association between radio and X-ray emission along the NE-SW radio axis and also that radio emission is not detected over the rest of the extent of the diffuse X-ray emission. This, together with the offset between the peaks of the X-ray and radio emissions may indicate that the jet axis in this source is precessing.

Key words: X-rays: individual: 3C 191, 3C 294 and 3C 432. galaxies: jets.

1 INTRODUCTION

Because to its unprecedented sensitivity and spatial resolution, *Chandra* has imaged a wide range of low- and high-redshift radio sources, revealing their detailed X-ray emission. Several processes can produce X-rays over large scales from these objects: thermal emission from shocks, as well as synchrotron radiation and inverse-Compton scattering of a seed photon field (e.g. Harris & Krawczynski (2002)). The latter can originate from a variety of sources. Synchrotron photons produced in the jet are up-scattered in the process known as Synchrotron Self-Compton (SSC). Thermal photons, reprocessed from the nuclear region, can be scattered into the jet (Scharf et al. 2003). A further source of photons is the Cosmic Microwave Background (CMB), which becomes more important with redshift (Felten & Rees 1969). All such photon fields, once up-scattered by the relativistic particles in the jet, produce spectra with the same spectral shape as the synchrotron radiation, because they scatter off the same population of electrons. If inverse-Compton is responsible for the X-ray emission, the radiative lifetimes of (highly energetic) radio synchrotron-emitting electrons are typically shorter than for the (less energetic) electrons which give inverse-Compton emission in the X-ray band, so inverse-Compton emission traces an older population of particles and may therefore be offset from, and less spatially compact than, the radio emission. For inverse-Compton scattering to dominate over synchrotron emission for a particular Lorentz factor γ, the magnetic field energy density must be less than the energy density of the seed photon field (i.e. $\frac{B^2}{8\pi} \leqslant \mathcal{U}_{\rm phot}$). Assuming that this criterion is met, the photon field with the highest energy density will be the most important source of inverse-Compton X-rays.

At redshift $z < 1$, the energy density of the CMB is low and inverse-Compton of the CMB (IC) emission is likely to be most important in sources only if the jets are relativistic (Tavecchio et al. 2000; Celotti et al. 2001). In sources that are not beamed, IC may be dominated by other X-ray emission processes (Sambruna et al. 2004). X-ray emission from an increasing number of jets and lobes at these redshifts has been detected and is often explained by IC (e.g. Sambruna et al. 2004, Harris & Krawczynski 2002, Belsole et al. 2004, Overzier et al. 2005 and Kataoka & Stawarz 2005). Some X-ray-bright jets appear to be closely aligned to the line-of-sight, relativistic and extending to distances of the order of $100\,{\rm kpc}$ (Tavecchio et al. 2004 and Marshall et al. 2005) and appearing, in some cases (e.g. MRC 1136-135, Sambruna et al. (2006)), to be systematically decelerating.

Since the energy density of the CMB increases as $(1+z)^4$, this counterbalances surface brightness dimming with redshift. Therefore, IC in powerful high-redshift objects should be detectable across the universe, even if beaming is not common (Schwartz 2002). So far, the search for IC in very high-redshift jets has proved elusive: current snapshot surveys of high-redshift

⋆ E-mail: mce@ast.cam.ac.uk

($z > 3.5$) radio-loud quasars have generally failed to detect extended X-ray jet emission (Bassett et al. 2004, Lopez et al. 2006 and Schwartz 2002).

This paper presents *Chandra* observations of two radio galaxies in the redshift range $1.75 - 2$ (3C 432 and 3C 191), with the aim of detecting and characterising their X-ray emission. These sources, and 3C 294 at $z = 1.786$ which is re-examined in this paper, are the highest redshift FR II radio galaxies (i.e. Fanaroff & Riley (1974) class II objects) to be detected in X-rays to date[1], with the exception of 6C 0905+3955 (Blundell et al. 2006) and 4C 41.17 (Scharf et al. 2003). New, deep radio observations of 3C 294 are also discussed. The galaxies were chosen because of their power and spatial extent, meaning that they have a large reservoir of relativistic particles resolvable by *Chandra* and so are ideal candidates in the search for IC. Preliminary reports of these results appear in Crawford (2006) and Erlund et al. (2006). Throughout this paper, all errors are quoted at 1σ unless otherwise stated and the cosmology is $H_0 = 71\,\mathrm{km\,s^{-1}\,Mpc^{-1}}$, $\Omega_0 = 1$ and $\Lambda_0 = 0.73$.

2 DATA REDUCTION

Table 1 contains a summary of source information and the X-ray observations analysed. The CIAO data processing software package was used for the X-ray data reduction (CIAO v3.2.2 and CALDB v3.1.0). Pixel randomisation was turned off for all observations using the *ACIS_PROCESS_EVENTS* tool and, when an observation had been taken in VFAINT mode, *check_vf_pha=yes* flag was set using the same tool. Then the Sub-pixel Resolution Algorithm (Tsunemi et al. 2001 and Mori et al. 2001) was used to make use of photons that arrive near the edges and corners of the pixels, as their arrival point can be determined with sub-pixel resolution. The algorithm adapts their positions accordingly. This improves the half power diameter (HPD) by approximately ten per cent without losing statistics or affecting spectral properties. Improving photon positioning improves the image quality, but not dramatically for these sources. Both 3C 191 and 3C 432 suffer from about 10 per cent pileup in the central source and the observations were taken in full frame mode with five chips.

In the case of 3C 191, Obs ID 2134 was reprojected onto the co-ordinates of 5626 and for 3C 294, Obs IDs 1588 and 3207 were reprojected onto the co-ordinates of 3445.

Spectra for the background (an area of sky free from sources near the target source and on the same chip), the central source, the extended X-ray emission and the extended X-ray emission lying within the radio contours were extracted separately for each observation and, when multiple observations were present, stacked using *XSPEC* v 11.3.2.

Despite the limited number of counts, the spectra were fitted with a Galactic absorbed power-law and, in the case of the nucleus, intrinsic absorption was also included in the model. χ^2-squared statistics were used to give a goodness of fit, while C-statistics, which is appropriate for low photon counts, were used to calculate errors. The results are presented in Table 3.

The radio observations were made with the VLA[2] in A-configuration on the dates listed in Table 2. The data were processed using standard techniques within the AIPS package, including self-calibration for phase only.

Source	frequency [GHz]	RMS noise [$\times 10^{-4}$ Jy/beam]	linear size [kpc]	Date
3C 191	8.46	1.11	40	2004 Sept. 18
3C 294	1.43	4.69	129	2001 Jan. 1
	8.46	0.66	129	1999 Aug. 13
3C 432	1.54	3.32	124	1992 Dec. 12

Table 2. All radio data were taken using the VLA in configuration A. RMS is the root mean squared of the background noise in the radio maps.

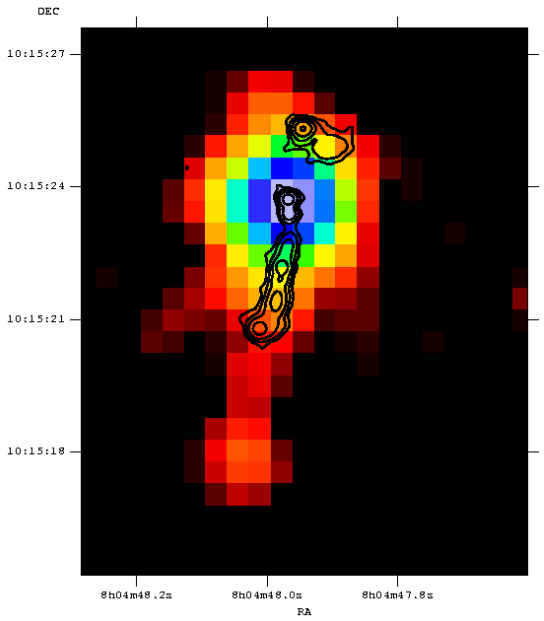

Figure 1. Gaussian-smoothed $0.5 - 3\,\mathrm{keV}$ X-ray image of 3C 191. The smoothing kernel was 1 pixel (0.49 arcsec). Overlaid are $8.46\,\mathrm{GHz}$ radio contours (0.4, 1.3, 4, 13, $40\,\mathrm{mJy/beam}$).

3 3C 191

3C 191 is a steep-spectrum, radio-loud, non-BAL (Broad Absorption Line) quasar with a central black hole of $\sim 10^9\,\mathrm{M_\odot}$ (**?**). High resolution spectroscopy has shown absorbing gas partially covering the central source: the absorption lines have flat-bottomed profiles, yet are fully resolved (Hamann et al. 2001). They are also blue-shifted between 400 and $1400\,\mathrm{km\,s^{-1}}$ and are consistent with an outflow with a flow-time of $\sim 3 \times 10^7$ years at a distance of $28\,\mathrm{kpc}$ from the quasar (Hamann et al. 2001). They seem to arise from a region of the outflow interacting with the disturbed ISM (Inter-Stellar Medium) in the elliptical host galaxy (Perry & Dyson 1990). The optical spectral index, $\alpha_{\mathrm{opt}} = 0.7$, indicates that there is little reddening along our line-of-sight to 3C 191; dust may have been destroyed in shocks due to the advancing radio source (Willott et al. 2002). 3C 191 has a residual rotation measure, which is defined as the rotation measure of the source minus the Galactic rotation measure in that direction, of $1700\,\mathrm{rad\,m^{-2}}$ (Kronberg et al. 1990). This is two orders of magnitude larger than other quasars with com-

[1] see http://hea-www.harvard.edu/XJET/index.cgi as of 2006 Jan 31

[2] The National Radio Astronomy Observatory is operated by Associated Universities, Inc., under cooperative agreement with the National Science Foundation.

Source	RA (J2000)	Dec (J2000)	z	kpc/ arcsec	$N_{H,G}$ cm^{-2}	Date	Obs ID	(V)FAINT	ks	Reference
3C 191	08h04m47.9s	+10d15m23s	1.956	8.493	2.28×10^{20}	2001 Mar. 7	2134	FAINT	8.32	Sambruna et al. (2004)
						2004 Dec. 12	5626	VFAINT	16.65	this paper
3C 294	14h06m44.0s	+34d11m25s	1.779	8.544	1.21×10^{20}	2000 Oct. 29	1588	FAINT	19.51	Fabian et al. (2001)
						2002 Feb. 25	3445	VFAINT	68.49	Fabian et al. (2003)
						2002 Feb. 27	3207	VFAINT	118.37	Fabian et al. (2003)
3C 432	21h22m46.2s	+17d04m38s	1.785	8.543	7.40×10^{20}	2005 Jan. 7	5624	VFAINT	19.78	this paper

Table 1. Source information: name, position, redshift, kpc at redshift of source per arcsec on the sky, Galactic absorption in the direction of the source. X-ray observation details: date of observation, *Chandra* OBSID, data mode, duration of flare-cleaned observations and references for published data.

Target	photons (bkgrd)	N_H 10^{21} cm^{-2}	Γ	L_X $(2-10\,\mathrm{keV})$ 10^{44} erg s^{-1}	χ^2_ν (dof) [ph/bin]
3C 191	ObsID: 2134 and 5626				
nucleus	247.96 (0.04); 599.88 (0.12)	$3.8^{+2.6}_{-2.8}$	$1.73^{+0.28}_{-0.12}$	$40.3^{+5.4}_{-0.9}$	0.66 (44) [15]
extended	21.96 (1.04) [8]*; 60.71 (1.29) [21]*	–	$1.63^{+0.36}_{-0.35}$	$2.33^{+0.65}_{-0.69}$	0.49 (4) [10]
		–	$1.56^{+0.13}_{-0.31}$	$2.40^{+0.54}_{-0.54}$	C-statistic
radio (8.46 GHz)	11.88 (0.12) [3]*; 27.85 (0.15) [7]*	–	$1.94^{+0.44}_{-0.21}$	$1.24^{+0.40}_{-0.41}$	C-statistic
3C 294†	ObsID: 1588, 3207 and 3445				
extended	92.73(10.27); 479.16 (60.84); 302.93 (32.07)	–	$2.08^{+0.11}_{-0.08}$	$2.93^{+0.15}_{-0.17}$	0.91 (60) [20]
radio (1.425 GHz)	44.88 (3.12); 215.42 (17.58); 136.73 (9.27)	–	$2.00^{+0.12}_{-0.11}$	$1.41^{+0.01}_{-0.10}$	0.54 (15) [20]
radio (8.46 GHz)	14.61 (0.39); 64.67 (2.33); 37.80 (1.20)	–	$1.98^{+0.43}_{-0.39}$	$0.41^{+0.11}_{-0.11}$	C-statistic
3C 432	ObsID: 5624				
nucleus	693.81 (0.19)	$0.21^{+0.36}_{-0.21}$	$1.84^{+0.09}_{-0.11}$	33.81	0.79 (36) [15]
extended	60.63 (1.37) [24]*	–	$1.53^{+0.35}_{-0.34}$	$1.77^{+0.54}_{-0.47}$	0.52 (5) [8]
		–	$1.57^{+0.27}_{-0.36}$	$1.85^{+0.45}_{-0.57}$	C-statistic
radio (1.54 GHz)	35.76 (2.24) [10]*	–	$1.52^{+0.27}_{-0.48}$	$1.37^{+0.49}_{-0.45}$	C-statistic

Table 3. Results of spectral fits.

Column 1: region analysed – extended region includes emission inside radio contours.
Column 2: contains the background subtracted number of source photons in region, in brackets is the number of background photons in region.
Column 3: the intrinsic absorption, which is only relevant to the nucleus of the source.
Column 4: photon index.
Column 5: X-ray luminosity in the $2-10$ keV band rest frame.
Column 6: the number not contained within brackets is the reduced-χ^2, the number of degrees of freedom is in round brackets and the number of photons per bin is in square brackets. The χ^2- and C-statistic values are consistent.
† A more complete analysis of 3C 294 can be found in Fabian et al. (2003) and has not been repeated here.
* Number of photons due to contamination from the central source PSF (i.e. added background). The L_X has been scaled accordingly.

parable radio morphology and is consistent with a thin shell of ~ 25 kpc across. The magnetic field parallel to the line-of-sight, calculated from this rotation measure, is $0.4-4\,\mu$G (Kronberg et al. 1990). This source is strongly optically variable. It has increased its nuclear X-ray luminosity by ~ 20 per cent between the two *Chandra* observations. It is possible that the nuclear X-rays are relativistically boosted, given the radio asymmetry and plausible projection.

The extended X-ray emission is preferentially aligned along the radio jet direction (Fig. 1) and, unusually, appears to continue well beyond the radio emission to the north and south. The X-ray emission spans 76 kpc; almost double that of the radio which is 40 kpc. The X-ray is extended by about 11 kpc to the north-east of the northern radio hot-spot: the radio emission goes in the opposite direction. The extended X-ray emission to the south is much more marked: it continues beyond the radio hot-spot by 32 kpc (3.75 arcsec). The photons at the very end of the X-ray jet seem to be grouped into a point-like source (hereafter referred to as the tail). This is not detected by *WAVDETECT* (a wavelet-transform procedure) which only finds the central source. In the snapshot Hubble Space Telescope (*HST*) data, there is neither an optical counterpart to the jet (Sambruna et al. 2004) nor the tail. It is not clear whether the tail is actually an extension of the jet or a coincidental source.

In order to characterise the tail, the jet is separated into sections: the extended emission to the north beyond the 3σ region of the central source as detected by *WAVDETECT*, hereafter referred to as the northern extension; the photons between the tail and the end of the 8.46 GHz jet (hereafter referred to as the southern bridge) and the tail. Considering only observation 5626 and ignoring contamination from the central source PSF, the tail (whose centroid appears to be separated from the rest of the jet by ~ 2 arcsec) contains 6 photons and has a hardness ratio of $+0.67^{+0.33}_{-0.49}$. The hardness ratio is a relationship between the number of photons in the hard (H) $2-8$ keV-band and in the soft (S) $0.5-2$ keV-band:

$\frac{H-S}{H+S}$, calculated using background subtracted counts. The southern bridge contains 14 photons and has a hardness ratio of $-0.76^{+0.32}_{-0.24}$ and the northern extension has 6 photons and a hardness ratio of $-1^{+0.58}_{-0.00}$. There seems to be a gradual change in hardness of the jet from soft to hard, although the photon statistics are not good enough to quantify this. Even if the tail were a coincidental source, the X-ray jet still extends beyond the 8.46 GHz radio emission. High resolution MERLIN data at 1.66 GHz follows the 8 GHz data very closely and is not more extended to the south.

X-ray synchrotron emission cannot be ruled out by the extrapolation of the radio flux in the jet up to X-ray wavelengths, assuming $\alpha \sim 1$ and an unbroken power-law; however, it is extremely unlikely that a single unbroken power-law could extend up to X-ray wavelengths. The radiative lifetimes would be extremely short, requiring constant re-acceleration along the full length of the radio jet. 3C 191 is not particularly luminous at IR wavelengths. It has not been detected by IRAS, and so only an upper limit of its 60 μm IR luminosity of $L_{\rm IR} < 4\times10^{46}$ erg s^{-1} is available. The energy density of the CMB, which is $\mathcal{U}_{\rm CMB} = 3.20 \times 10^{-11}$ erg cm^{-3}, will dominate over the energy density in IR photons at ~ 30 kpc, but it should be remembered that this is an upper limit. The X-ray emission aligned along the jet axis is much more extended and so cannot be explained by up-scattering of nuclear IR photons. It is also possible for nuclear radiation to be the dominant inverse-Compton seed photon field. Both the optical quasar luminosity of $L_{\rm nucl} = 2.69 \times 10^{46}$ erg s^{-1} (Sandage et al. 1965), presumably produced by accretion, and the luminosity of the Broad Line Region (BLR), which typically constitutes the dominant scattered field for relativistic jets on sub-pc scales, $\rm L_{BLR} = 1.7 \times 10^{46}$ erg s^{-1}(**?**), are likely to be less important. They would be dominated by $\mathcal{U}_{\rm CMB}$ at 27 kpc from the nucleus, which is the size of the extended central source region seen in Fig. 1 and is at roughly the same distance as the outflowing shell inferred from other wavelength observations. X-rays are detected along the full length of the radio jet and beyond, which implies that they are not generated by SSC. The extent of the X-ray emission therefore favours IC, as does the detection of photons beyond the end of the jet.

A plausible explanation as to why we detect X-rays beyond the end of the radio jet is that 3C 191 could be a double-double radio source whose jet has been interrupted and restarted (Schoenmakers et al. 2000), possibly by the same mechanism responsible for the large-scale outflow detected by Hamann et al. (2001), which is thought to be 30 Myr old. This is long enough for the original radio emission (especially at 8.46 GHz) to no longer be observable. IC is preferentially emitted from aged plasma as clearly demonstrated by 6C 0905+3955, where X-rays are visible along the length of the jet emanating from aged plasma, which is no longer emitting in the radio (Blundell et al. 2006). So IC X-rays provide an excellent tracer of aged synchrotron plasma, and observations of double-double radio sources would be an interesting demonstration of this with a combination of X-ray and radio observations. It should also be noted that the 8.46 GHz jet emission is only 40 kpc-long which is consistent with it being very young (note that this is the projected length and that this quasar is one-sided).

4 3C 294

3C 294 is a powerful FR II radio galaxy with an intriguingly shaped radio jet (Fig. 5) which is highly depolarised, indicating that it lies within a dense medium. It is embedded in a luminous Lyman-α (Lyα) halo, which has a large velocity shear and is roughly aligned

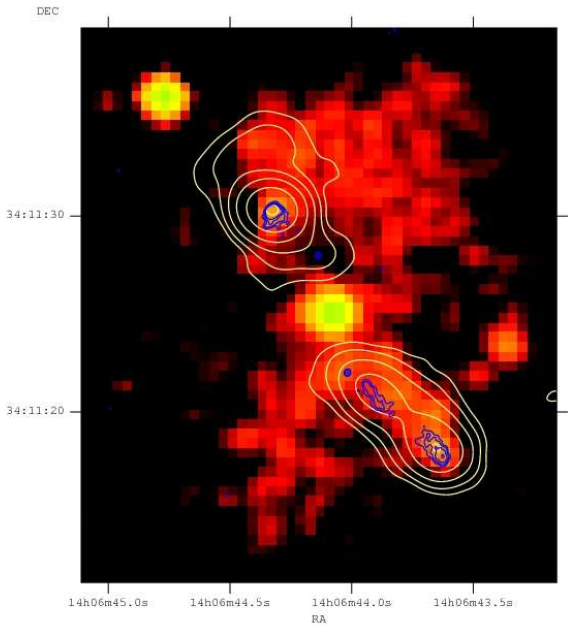

Figure 2. Gaussian-smoothed $0.5 - 3$ keV X-ray image of all three observations of 3C 294. The smoothing kernel was 1 pixel. Overlaid with 8.46 GHz radio contours in blue (0.24, 1.1, 5.2, 24 mJy/beam) and yellow 1.425 GHz radio contours (0.002, 0.006, 0.02, 0.06, 0.2, 0.6 Jy/beam).

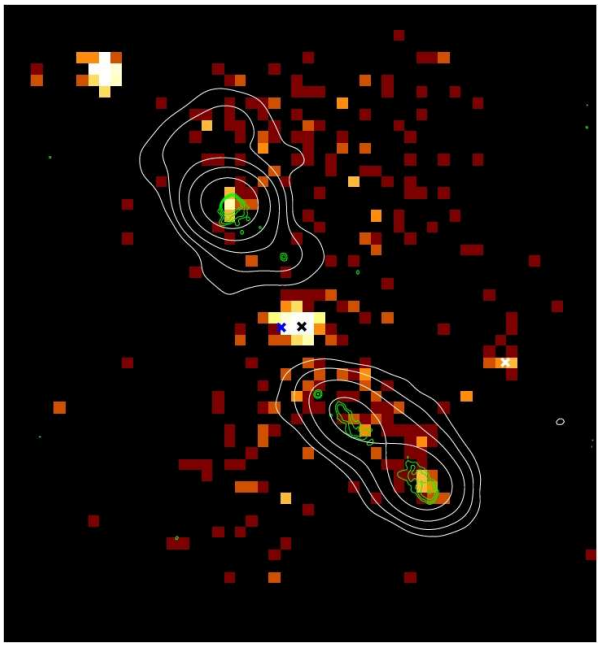

Figure 3. $0.5 - 7$ keV X-ray image of 3C 294. Overlaid with 8.46 GHz radio contours in green (0.24, 1.1, 5.2, 24 mJy/beam) and white 1.425 GHz radio contours (0.002, 0.006, 0.02, 0.06, 0.2, 0.6 Jy/beam). The eastern-most cross represents, in dark blue, the location of Stockton et al. (2004) eastern stellar object, the central cross, in black, is at the position of the radio core and western-most cross, in white, represents the position for the AO star. All three postitions are taken from Stockton et al. (2004).

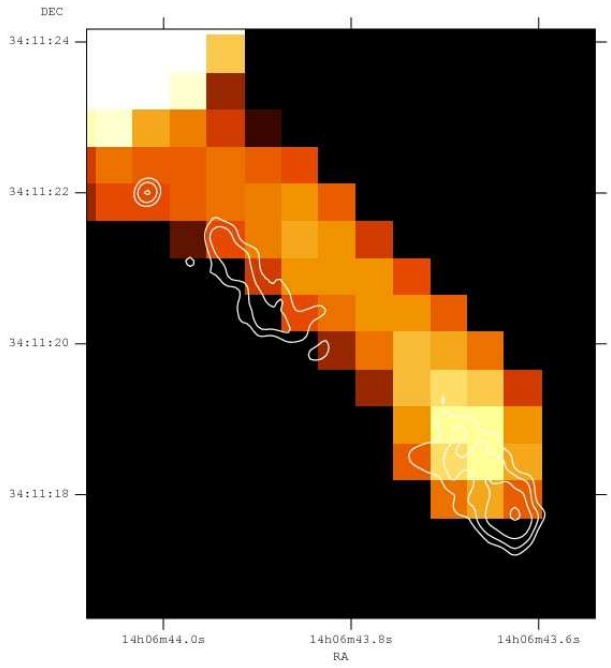

Figure 4. Gaussian-smoothed $0.5 - 3\,\mathrm{keV}$ X-ray image. The smoothing kernel was 2 pixels. Overlaid with $8.46\,\mathrm{GHz}$ (0.24, 0.40, 0.67, $1.1\,\mathrm{mJy/beam}$). The contrast has been adjusted to highlight the significant offset between the X-ray and radio jet emission.

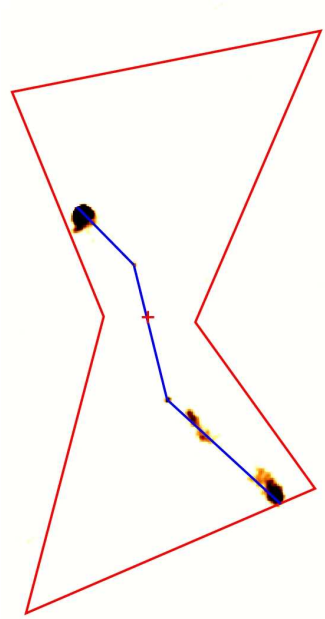

Figure 5. This schematic shows the outline of the the extended X-ray emission in red, with a red cross marking the X-ray nucleus. Overlaid on the $8\,\mathrm{GHz}$ radio image are blue lines showing how the jet has changed its orientation.

with the radio source direction. This gas requires a mass equivalent to present day massive elliptical galaxies and their halos in order for the system to be gravitationally bound (McCarthy et al. 1990). An over-density of red galaxies has also been detected in the near infrared (NIR) in a $2' \times 2'$ field around 3C 294 (Toft et al. 2003). Stockton et al. (2004) have carried out high spatial resolution infrared imaging and find the central nucleus to have two distinct cores separated by an arcsecond. Both appear to be Active Galactic Nuclei (AGN); one is compact and dominated by light from an old stellar population, the other is more diffuse and contains the principle X-ray core. The latter, a partially obscured AGN, has both a reflection component and a redshifted $6.4\,\mathrm{keV}$ iron line (Fabian et al. 2003). Another AGN, consistent with being at the same redshift as 3C 294, is $104\,\mathrm{kpc}$ to the north-east of 3C 294.

Bright X-ray emission associated with the NE-SW radio axis is clearly detected. The X-ray emission is slightly offset and rotated with respect to the radio emission, as can be seen in Fig. 2 and Fig. 4. The X-ray emission is much more extended than the radio emission, even in the deeper radio observations presented here. In fact, careful inspection of both the $1.425\,\mathrm{GHz}$ and $8.46\,\mathrm{GHz}$ radio data shows no radio emission along the NW-SE axis of the X-ray source. Fabian et al. (2003) showed that the surface brightness profile of this diffuse, hour-glass-shaped emission declines very steeply at the edges, making it unlikely to be due to thermal emission: it is best modelled as IC.

Fig. 5 shows that the high frequency radio emission to the north-east and south-west lie parallel to each other. This favours a change in jet direction due to a change in direction from the nucleus or a shearing of the radio jet by the ambient medium, rather than due to a change in ambient pressure (McCarthy et al. 1990). The hour-glass X-ray morphology, together with the current jet axis as seen in the radio, supports the idea of a precessing jet, such as that found in the microquasar SS433 (Blundell & Bowler 2004). This is because the lifetime of IC electrons is more than an order of magnitude longer than those responsible for the $8.46\,\mathrm{GHz}$ radio emission and, assuming that the synchrotron number density power-law continues down to these lower Lorentz factors, there will also be more IC electrons. The lifetime of the extended inverse-Compton X-ray emission suggests a precession timescale of $>\sim 10^7\,\mathrm{yr}$. Note that the double nucleus may favour a precession model (Stockton et al. 2004).

The astrometry of the three observations was corrected using the Aspect Calculator.[3] Figure 3 shows the raw image with crosses marking the position of central core, the eastern stellar object (identified by Stockton et al. (2004)) and the position of the AO star (all positions were taken from Stockton et al. (2004)), all of which match their X-ray counterparts well. The northern X-ray hotspot clearly coincides with the $8\,\mathrm{GHz}$ radio hotspot. The peak of the X-ray emission associated with the southern radio hotspot appears to lie behind the radio hotspot (see also Fig. 4), but this is within the errors of *Chandra*'s $0.6\,\mathrm{arcsec}$ positional uncertainty. To the south, the bulk of the X-ray emission lies to the north of the $8\,\mathrm{GHz}$ emission, running roughly parallel to the southern radio jet and matching the radio features. The offset between the X-ray and radio jet is $\sim 1\,\mathrm{arcsec}$ (as illustrated in Fig. 4). This adds weight to the idea that 3C 294 is precessing because it appears that the bulk of the X-ray emission comes from where the jet was, and not where it now is. This is another example of X-rays being emitted from old plasma as is the case for 3C 191 and 6C 0905+3955.

5 3C 432

3C 432 is a powerful, lobe-dominated, FR II radio quasar. There is a moderate depolarisation asymmetry (Fernini 2001) demonstrating

[3] at http://cxc.harvard.edu/cal/ASPECT/fix_offset/fix_offset.cgi

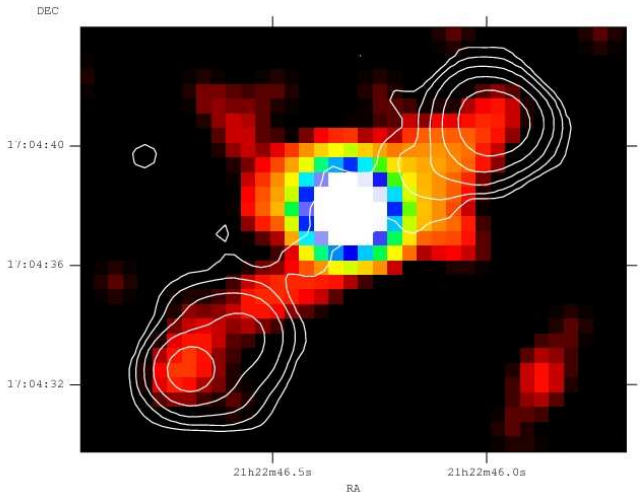

Figure 6. Gaussian-smoothed $0.5-3\,\mathrm{keV}$ X-ray image of 3C 432. The smoothing kernel was 1.5 pixels ($0.74\,\mathrm{arcsec}$). Overlaid with $1.54\,\mathrm{GHz}$ radio contours (0.001, 0.0035, 0.012, 0.042, $0.144\,\mathrm{Jy/beam}$).

that, like many FR II sources, it is surrounded by a Faraday-thick magneto-ionic medium (Laing 1988; Garrington et al. 1988). The central black hole has a mass of $\sim 5\times10^9\,\mathrm{M}_\odot$ as inferred from Mg II line-widths (**?**).

The radio spectral index [$S_\nu \propto \nu^{-\alpha}$] is $\alpha_R = 0.98$ in the MHz-band[4], steepening to $\alpha_R = 1.20$ in the GHz-band (Richards et al. 2001). The X-ray energy spectral index α_X is found from the X-ray photon index Γ in Table 3 using $\alpha = \Gamma - 1$; $\alpha_\mathrm{X} \sim 0.8$ for the nuclear region and $\alpha_\mathrm{X} \sim 0.5$ for the extended region.

Fig. 6 shows a Gaussian-smoothed image of 3C 432; apart from two spurs, one to the east and one to the west of the nucleus (possibly due to readout streaks from pile-up in the central source), the X-ray emission is contained within the $1.54\,\mathrm{GHz}$ radio contours.

X-ray emission due to synchrotron radiation cannot be ruled out from an extrapolation of the radio flux, assuming $\alpha \sim 1$ and a single, unbroken power-law. The radiative lifetime of these electrons would be of the order of several hundred years assuming a typical magnetic field, meaning that even if the electrons were re-accelerated sufficiently in the hot-spot, they would not be detectable throughout the lobe: a lifetime of $> 10^5\,\mathrm{yr}$ is necessary for the electrons to have the time to travel to their detected locations. Synchrotron emission can be ruled out unless the electrons are being continuously re-accelerated throughout the whole of the radio lobe: it is hard to think of a feasible physical theory which would allow this (Blundell & Rawlings 2000). The double-sided nature of the X-ray emission in this source argues against Doppler beaming from a jet.

There are not enough photons to constrain a thermal spectrum, so a thermal model cannot formally be rejected. On the assumption that 3C 432 is lobe dominated, the X-rays are not produced in shocks along the jet. They must be produced by inverse-Compton up-scattering of a seed photon field. SSC is important in compact sources, such as at the base of the jet or the hot-spots, so this process is disfavoured by the extended nature of the X-ray emission throughout lobe. Another possible seed photon field is the IR photon field from the nuclear region. 3C 432 has not been detected by IRAS so only upper limits on the $60\,\mu\mathrm{m}$ luminosity of $L_\mathrm{IR} < 3\times10^{46}\,\mathrm{erg\,s^{-1}}$ exists. (Neugebauer et al. 1986). The energy density of the CMB is $\mathcal{U}_\mathrm{CMB} = 2.52\times10^{-11}\,\mathrm{erg\,cm^{-3}}$ at the redshift of 3C 432. So the CMB will be the dominant photon field beyond $\sim 30\,\mathrm{kpc}$, although this is only an upper limit. A better constrained photon field, but one which is likely to be less important in unbeamed sources such as this one, is the luminosity from the accretion process in the active nucleus, and that of the BLR. The latter is estimated at $3.7\times10^{45}\,\mathrm{erg\,s^{-1}}$ (**?**), and thus a typical value for the former would be ten times higher (for a BLR covering factor ~ 0.1). The CMB will dominate over these photon fields beyond $\sim 35\,\mathrm{kpc}$ which means that it will dominate in the radio lobes in Fig. 6. The X-ray emission extends well beyond the influence of these two nuclear photon fields: 3C 432 is $124\,\mathrm{kpc}$-long. The extent of the X-rays favours IC of the CMB in this relatively high redshift source.

6 ENERGY ARGUMENTS

Radio galaxies are thought to trace massive galaxies as they are often associated with large pools of line-emitting gas comparable to the envelopes of local cD galaxies (van Ojik et al. 1997). Some high-redshift radio galaxies have been associated with proto-clusters (including 3C 294). Extreme Faraday-rotation measures, similar to those found in local clusters, along with over-densities of Hα-emitters, Lyα-emitters and EROs (Extremely Red Objects), all of which imply a typical cluster environment, are not confirmed by X-ray observations. Such systems may not be virialised structures, so the gaseous environments are not in a deep enough potential well to emit in the X-ray-band. At low redshifts ($z < 0.1$), radio-loud quasars are preferentially found in galaxy groups and poor-to-moderate clusters (Best 2004). Away from the X-rays associated with lobes and hot-spots, soft thermal emission is often detected with bolometric luminosities of a few times $10^{43}\,\mathrm{erg\,s^{-1}}$, extending over a few hundred kiloparsecs at the redshift of the quasar (Crawford & Fabian 2003). The influence of radio galaxies on the gaseous properties of a poor cluster environment would steepen the $L_\mathrm{X} - T_\mathrm{X}$ relationship and so high-redshift powerful radio galaxies may be in the epoch of pre-heating the proto-cluster environment. It is therefore important to discover the amount of energy contained in the jets and lobes of such galaxies.

A lower limit to the amount of energy stored in electrons can be calculated by assuming that the X-ray emission detected is indeed due to IC.

The rate at which one electron loses energy in an isotropic radiation field depends on the energy, ϵ_ph, of the photons to be up-scattered, the Lorentz factor of the electron γ_e squared, which is roughly the amount by which inverse-Compton scattering boosts the initial photon energy, and the rate at which the interaction takes place. This is given by the Thomson cross-section, σ_T, times the speed of light, c, times the number density of photons available, n_ph. $\mathcal{U}_\mathrm{rad}$ is the energy density of the photon seed field. The rate of energy loss is therefore given by:

$$\frac{d\mathcal{E}}{dt} = n_\mathrm{ph}\frac{4}{3}\gamma_\mathrm{e}^2\epsilon_\mathrm{ph}\sigma_\mathrm{T}c = \mathcal{U}_\mathrm{rad}\frac{4}{3}\gamma_\mathrm{e}^2\sigma_\mathrm{T}c. \quad (1)$$

The sources studied here are assumed not to be beamed and to have a negligible k-correction. On the assumption that CMB photons only scatter off relativistic electrons with Lorentz factor $\gamma_\mathrm{e} \sim 10^3$, these electrons can be represented as a δ-function rather

[4] http://www.3crr.dyndns.org/cgi/sourcepage?15

than the standard power-law distribution. This δ-function of electrons, when scattering the black-body spectrum of CMB photons, produces the $2-10\,\mathrm{keV}$-band detected rest-frame X-ray luminosity. This is also given by multiplying Equation (1) by the number density of electrons, N_e with γ_e

$$L_\mathrm{X} = N_\mathrm{e}\mathcal{U}_\mathrm{rad}\frac{4}{3}\gamma_\mathrm{e}^2\sigma_\mathrm{T}c. \quad (2)$$

The energy in these relativistic electrons is $\mathcal{E}_\mathrm{e}$

$$\mathcal{E}_\mathrm{e} = N_\mathrm{e}\gamma_\mathrm{e}m_\mathrm{e}c^2, \quad (3)$$

where m_e is the rest mass of the electron. Re-arranging Equation (2) to give an expression for N_e and substituting it into Equation (3) gives

$$\mathcal{E}_\mathrm{e} = \frac{3}{4}\frac{L_\mathrm{X}m_\mathrm{e}c}{\mathcal{U}_\mathrm{rad}\gamma_\mathrm{e}\sigma_\mathrm{T}} \simeq \frac{3}{4}\frac{L_{44}}{\gamma_\mathrm{e}(1+z)^4}10^{64}, \quad (4)$$

where $L_\mathrm{X} = L_{44}\times10^{44}\,\mathrm{erg\,s^{-1}}$ and $\mathcal{E}_\mathrm{e}$ is in erg. The results of this calculation for 3C 432, 3C 191 and 3C 294 are presented in Table 4. These sources have a redshift of $z\sim2$: the minimum energy in relativistic particles with $\gamma\sim10^3$ will therefore be of the order of 10^{59} erg. This lower limit is important because IC electrons are longer-lived than their radio-synchrotron-producing counterparts, giving a better indication of the longevity of the source and the total energy it injects into its surroundings, which may have implications for understanding galaxy formation.

The above estimate is strictly a lower limit, as it assumes a monochromatic (narrow) electron energy distribution. Assuming that the electrons responsible for the X-ray emission are from an electron population which follows a standard power-law $N(\gamma) = N_0\gamma^{-p}$, then the energy E originally contained in these electrons is given by

$$E = \int_{\gamma_\mathrm{min}}^{\gamma_\mathrm{max}} N(\gamma)\gamma m_\mathrm{e}c^2 d\gamma, \quad (5)$$

where N_0 is the normalisation of the power-law. γ_min and γ_max are the minimum and maximum Lorentz factors assumed to be present in the jet and $p = 2\alpha+1 = 2\Gamma-1$. Here, α is the X-ray spectral index and Γ is the X-ray photon index from the X-ray data fits which are listed, along with L_X, in Table 3.

L_X is the integrated inverse-Compton flux, assuming a monochromatic distribution of CMB photons, and can be used to determine N_0:

$$L_\mathrm{X} = \frac{(4/3)^\alpha}{2}N_0\sigma_T c\frac{aT_{CMB}^4}{\nu_{CMB}^{1-\alpha}}\frac{\nu_2^{1-\alpha}-\nu_1^{1-\alpha}}{1-\alpha}, \quad (6)$$

where $h\nu_{CMB} = kT_{CMB}$. If $\Gamma\sim2$ (as is the case for 3C 294) then Equation 6 will be replaced by

$$L_\mathrm{X} = \frac{(4/3)^\alpha}{2}N_0\sigma_T c\frac{aT_{CMB}^4}{\nu_{CMB}^{1-\alpha}}\ln\frac{\nu_2}{\nu_1},$$

where ν_1 and ν_2 are the frequencies in Hz at 2 keV and 10 keV in the rest-frame respectively. It assumes that end points of the electron distribution do not contribute and that the Thomson limit criterion ($\sqrt{\frac{h\nu}{k_\mathrm{b}T}} \ll m_\mathrm{e}c^2$) is upheld, which are both the case over the range in γ of electrons responsible for up-scattering the CMB. T is the temperature of the CMB at the redshift of the source, given by $T = T_\mathrm{CMB}(1+z)$, where $T_\mathrm{CMB} = 2.728\,\mathrm{K}$ is the temperature of the CMB at $z=0$. h is Planck's constant and k_b is the Boltzmann constant.

Note that this calculation does not require equipartition to be assumed because the X-ray emission is used to constrain the power-law normalisation. This calculation is, however, highly sensitive to the value of the X-ray photon index, Γ, and its errors, as well as depending on the choice of γ_min and γ_max which are poorly constrained values. When $\gamma_\mathrm{min} = 10^3$, $\gamma_\mathrm{max} = 10^5$ and $\Gamma = 1.7$ are chosen, one obtains $E\sim1.5\mathcal{E}_\mathrm{e}$.

Target	radio structure [a] [GHz]	$\mathcal{E}_e$ [b] [$\times10^{59}$ erg]	B_max [μG]
3C 432	1.54	1.81 ± 0.93	25
	ext	2.44 ± 1.14	
3C 191	4.85	$1.29.\pm0.65$	28
	ext	2.50 ± 1.08	
3C 294	8.46	0.55 ± 0.25	25
	1.425	1.88 ± 0.79	
	ext	3.91 ± 1.42	

Table 4. The C-statistic values of L_X in Table 3 were used to calculate $\mathcal{E}_e$. The errors on $\mathcal{E}_\mathrm{e}$ were found by sampling a Gaussian distribution about L_X with a standard deviation of the average of the errors on L_X and sampling γ_e from a log-normal distribution about 10^3. [a] ext refers to all the extended X-ray emission, both within and outside of the radio contours. [b] 10^6 trials were used to calculate the errors on $\mathcal{E}_\mathrm{e}$.

So far, only the energy originally in a power-law population of relativistic electrons has been taken into account. There is a considerable amount of debate about the composition of the jet and this uncertainty can be represented by a factor k, $E_\mathrm{tot} = kE$. k can range from $k\sim\mathcal{O}(1)$ for a purely electron-positron jet, and the energy in the jet is that calculated above, to $k\sim\mathcal{O}(1000)$ for purely electron-proton jets (for cold protons). A growing body of work supports the idea of a mainly electron-positron jet (e.g. Reynolds et al. 1996 and Dunn & Fabian 2004), although, arguments for mainly electron-proton jets can be found in Celotti & Fabian (1993) and in Sikora et al. (2005); the latter work argues for a proton-dominated jet where the number of electron-positron pairs greatly exceeds the number of protons in high-power jets typical of FR II sources. Any entrainment of material surrounding the jet and/or lobe would also alter the value of k (e.g. for radio sources in clusters: Fabian et al. 2002 and Dunn et al. 2005).

If the choice of γ_min and γ_max were correct for the power-law before it was adiabatically expanded, then the energy in relativistic electrons calculated here would be an under-estimate; note also that we do not take into account any pdV work done on any surrounding medium. An originally unbroken power-law is assumed and is justifiable because we would like to know the energy that was originally in the electron population before any energy losses occurred. This estimate does not take into account possible re-acceleration, so would be an under-estimate if the same electrons which, having cooled once, were re-accelerated and enabled to cool again.

The dominant radiation mechanism, synchrotron or IC, for the electrons with $\gamma\sim10^3$ depends on the energy density of the magnetic field, $\mathcal{U}_\mathrm{B}$, compared to that of the CMB, $\mathcal{U}_\mathrm{CMB}$. If $\mathcal{U}_\mathrm{B}\sim\mathcal{U}_\mathrm{CMB}$, then the electrons thought to be responsible for up-scattering the CMB would in fact emit at low synchrotron frequencies. Therefore, in assuming that electrons with $\gamma\sim10^3$ efficiently cool via IC producing the X-rays detected, this places an upper-limit on the magnetic field, B_max, which is given by (Schwartz 2002):

$$B_\mathrm{max} = (z+1)^2T_\mathrm{CMB}^2(8\pi\mathrm{a})^{\frac{1}{2}}, \quad (7)$$

where the radiation density constant is $a = 7.5646\times10^{-15}\,\mathrm{erg\,cm^{-3}\,K^{-4}}$. This puts a constraint on the magnetic field

energy density which, together with the energy contained in particles, gives the total energy in the jet (Fabian et al. 2002):

$$E_{\rm jet} = kE + Vf\frac{B^2}{8\pi} = kE + E_{\rm B}, \quad (8)$$

where f is the volume filling fraction and V is the volume of the lobe. Assuming $f = 1$, V is a cylinder on the sky whose diameter and length are the dimensions of the extracted regions for extended X-ray emission. This is an over-estimate of the volume, and thus of the total energy in the magnetic field. Nonetheless, for both 3C 432 and 3C 191, the energy in the particles responsible for the X-ray emission, $\mathcal{E}_{\rm e}$, which is a robust lower limit to the energy stored in relativistic particles in the jet, is roughly a factor of two greater than the energy in the magnetic field, $E_{\rm B}$. For 3C 294, where the volume V is represented by two cones, $E_{\rm B} \sim \mathcal{E}_{\rm e}$. This means that the energy stored in relativistic particles E is greater than that stored in the magnetic field, $E_{\rm B}$. An important caveat is that we assumed that the emission from these jets is not dominated by relativistic bulk motion; if it was then the estimated particle number could dramatically change.

7 CONCLUSIONS

The *Chandra* observations of two relatively high-redshift FR II radio galaxies, 3C 432 and 3C 191, show extended X-ray emission which is most convincingly explained by inverse-Compton scattering of CMB photons. 3C 191 appears to produce X-ray emission from beyond the end of the radio jet, which appears to be harder than the rest of the extended emission. The possibility of a coincidental background or foreground source cannot be excluded.

New radio data for 3C 294 is presented, confirming the results from Fabian et al. (2003) and illustrating that the X-ray emission is much more extended than the radio emission. This and the offset detected between the radio jet axis, which represents current jet activity and the X-ray emission, which traces the jet's previous position, provides some evidence that this source is precessing.

The X-ray luminosity of the extended regions of these sources is used to calculate the energy contained in the electrons responsible for the X-ray emission. This gives a lower limit to the amount of energy in the lobe of the order of a few times 10^{59} erg if X-ray producing electrons are assumed to have a Lorentz factor $\gamma \sim 10^3$. The energy estimate increases by a factor of ~ 1.5 when a power-law distribution of electrons is considered and possibly by up to 10^3 when the proton component is included.

ACKNOWLEDGEMENTS

MCE acknowledges PPARC for financial support. ACF, CSC and KMB thank the Royal Society. AC acknowledges the Italian MIUR for financial support. We also thank the referee for their helpful comments.

REFERENCES

Bassett L. C., Brandt W. N., Schneider D. P., Vignali C., Chartas G., Garmire G. P., 2004, AJ, 128, 523
Belsole E., Worrall D. M., Hardcastle M. J., Birkinshaw M., Lawrence C. R., 2004, MNRAS, 352, 924
Best P. N., 2004, MNRAS, 351, 70
Blundell K. M., Bowler M. G., 2004, ApJ, 616, L159
Blundell K. M., Fabian A. C., Crawford C. S., Erlund M. C., Celotti A., 2006, ApJ, 644, L13
Blundell K. M., Rawlings S., 2000, AJ, 119, 1111
Celotti A., Fabian A. C., 1993, MNRAS, 264, 228
Celotti A., Ghisellini G., Chiaberge M., 2001, MNRAS, 321, L1
Crawford C. S., 2006, Astronomische Nachrichten, 327, 191
Crawford C. S., Fabian A. C., 2003, MNRAS, 339, 1163
Dunn R. J. H., Fabian A. C., 2004, MNRAS, 355, 862
Dunn R. J. H., Fabian A. C., Taylor G. B., 2005, MNRAS, 364, 1343
Erlund M. C., Fabian A. C., Blundell K. M., Celotti A. C., Crawford C. S., 2006, in Wilson A., ed, Proceedings of the 'The X-ray Universe 2005', p. 611
Fabian A. C., Celotti A., Blundell K. M., Kassim N. E., Perley R. A., 2002, MNRAS, 331, 369
Fabian A. C., Crawford C. S., Ettori S., Sanders J. S., 2001, MNRAS, 322, L11
Fabian A. C., Sanders J. S., Crawford C. S., Ettori S., 2003, MNRAS, 341, 729
Fanaroff B. L., Riley J. M., 1974, MNRAS, 167, 31P
Felten J. E., Rees M. J., 1969, Nat, 221, 924
Fernini I., 2001, AJ, 122, 83
Garrington S. T., Leahy J. P., Conway R. G., Laing R. A., 1988, Nat, 331, 147
Hamann F. W., Barlow T. A., Chaffee F. C., Foltz C. B., Weymann R. J., 2001, ApJ, 550, 142
Harris D. E., Krawczynski H., 2002, ApJ, 565, 244
Kataoka J., Stawarz Ł., 2005, ApJ, 622, 797
Kronberg P. P., Zukowski E. L. H., Perry J. J., 1990, ApJ, 355, L31
Laing R. A., 1988, Nat, 331, 149
Lopez L. A., Brandt W. N., Vignali C., Schneider D. P., Chartas G., Garmire G. P., 2006, AJ, 131, 1914
Marshall H. L. et al., 2005, ApJS, 156, 13
McCarthy P. J., Spinrad H., Dickinson M., van Breugel W., Liebert J., Djorgovski S., Eisenhardt P., 1990, ApJ, 365, 487
Mori K., Tsunemi H., Miyata E., Baluta C. J., Burrows D. N., Garmire G. P., Chartas G., 2001, in ASP Conf. Ser. 251: New Century of X-ray Astronomy, p. 576
Neugebauer G., Miley G. K., Soifer B. T., Clegg P. E., 1986, ApJ, 308, 815
Overzier R. A., Harris D. E., Carilli C. L., Pentericci L., Röttgering H. J. A., Miley G. K., 2005, A&A, 433, 87
Perry J. J., Dyson J. E., 1990, ApJ, 361, 362
Reynolds C. S., Fabian A. C., Celotti A., Rees M. J., 1996, MNRAS, 283, 873
Richards G. T., Laurent-Muehleisen S. A., Becker R. H., York D. G., 2001, ApJ, 547, 635
Sambruna R. M., Gambill J. K., Maraschi L., Tavecchio F., Cerutti R., Cheung C. C., Urry C. M., Chartas G., 2004, ApJ, 608, 698
Sambruna R. M., Gliozzi M., Donato D., Maraschi L., Tavecchio F., Cheung C. C., Urry C. M., Wardle J. F. C., 2006, ApJ, 641, 717
Sandage A., Véron P., Wyndham J. D., 1965, ApJ, 142, 1307
Scharf C., Smail I., Ivison R., Bower R., van Breugel W., Reuland M., 2003, ApJ, 596, 105
Schoenmakers A. P., de Bruyn A. G., Röttgering H. J. A., van der Laan H., Kaiser C. R., 2000, MNRAS, 315, 371
Schwartz D. A., 2002, ApJ, 569, L23
Sikora M., Begelman M. C., Madejski G. M., Lasota J.-P., 2005, ApJ, 625, 72

Stockton A., Canalizo G., Nelan E. P., Ridgway S. E., 2004, ApJ, 600, 626
Tavecchio F., Maraschi L., Sambruna R. M., Urry C. M., 2000, ApJ, 544, L23
Tavecchio F., Maraschi L., Sambruna R. M., Urry C. M., Cheung C. C., Gambill J. K., Scarpa R., 2004, ApJ, 614, 64
Toft S., Pedersen K., Ebeling H., Hjorth J., 2003, MNRAS, 341, L55
Tsunemi H., Mori K., Miyata E., Baluta C., Burrows D. N., Garmire G. P., Chartas G., 2001, ApJ, 554, 496
van Ojik R., Roettgering H. J. A., Miley G. K., Hunstead R. W., 1997, A&A, 317, 358
Willott C. J., Rawlings S., Archibald E. N., Dunlop J. S., 2002, MNRAS, 331, 435